Molecules and Cells

Crystal Structure of the Regulatory Domain of AphB from *Vibrio vulnificus*, a Virulence Gene Regulator

Nohra Park[1,3], Saemee Song[1,3], Garam Choi[1,2], Kyung Ku Jang[1,2], Inseong Jo[1], Sang Ho Choi[1,2,*], and Nam-Chul Ha[1,*]

[1]Department of Agricultural Biotechnology, Center for Food Safety and Toxicology, and Research Institute for Agriculture and Life Sciences, Seoul National University, Seoul 08826, Korea, [2]National Research Laboratory of Molecular Microbiology and Toxicology, Seoul National University, Seoul 08826, Korea, [3]These authors contributed equally to this work.
*Correspondence: choish@snu.ac.kr (SHC); hanc210@snu.ac.kr (NCH)
http://dx.doi.org/10.14348/molcells.2017.0015
www.molcells.org

The transcriptional activator AphB has been implicated in acid resistance and pathogenesis in the food borne pathogens *Vibrio vulnificus* and *Vibrio cholerae*. To date, the full-length AphB crystal structure of *V. cholerae* has been determined and characterized by a tetrameric assembly of AphB consisting of a DNA binding domain and a regulatory domain (RD). Although acidic pH and low oxygen tension might be involved in the activation of AphB, it remains unknown which ligand or stimulus activates AphB at the molecular level. In this study, we determine the crystal structure of the AphB RD from *V. vulnificus* under aerobic conditions without modification at the conserved cysteine residue of the RD, even in the presence of the oxidizing agent cumene hydroperoxide. A cysteine to serine amino acid residue mutant RD protein further confirmed that the cysteine residue is not involved in sensing oxidative stress in vitro. Interestingly, an unidentified small molecule was observed in the inter-subdomain cavity in the RD when the crystal was incubated with cumene hydroperoxide molecules, suggesting a new ligand-binding site. In addition, we confirmed the role of AphB in acid tolerance by observing an *aphB*-dependent increase in *cadC* transcript level when *V. vulnificus* was exposed to acidic pH. Our study contributes to the understanding of the AphB molecular mechanism in the process of recognizing the host environment.

Keywords: crystal structure, low pH, transcriptional regulator AphB, *vibrio vulnificus*

INTRODUCTION

Many pathogenic bacteria increase the expression of virulence factors by recognizing and responding to the host environment. *Vibrio vulnificus* is a facultative aerobic gram-negative species that lives in marine environments and in the human body (Horseman and Surani, 2011; Lee et al., 2014). Oral ingestion of food contaminated with *V. vulnificus* or direct administration of the bacteria to injured skin can cause acute gastroenteritis or invasive septicemia, respectively. Once in the human host, the bacteria can rapidly expand by sensing the human environment. *V. vulnificus* produces toxins during the pathogenic response, whose gene expression is governed by global regulators that recognize the host environments (Lee et al., 2014).

Vibrio cholerae, closely related to *V. vulnificus*, activates the ToxR virulence cascade, which is initiated by two transcriptional regulators: the winged-helix AphA and the LysR family transcriptional regulator (LTTR) AphB. The active form of AphB binds to the *tcpPH* promoter and induces its transcription by cooperating with AphA. TcpPH functions coop-

Received 2 February, 2017; revised 5 April, 2017; accepted 7 April, 2017; published online 20 April, 2017

eISSN: 0219-1032

eratively with ToxR in the virulence signaling pathway by expression of ToxT, a major regulator of virulence factor transcription in *V. cholerae* (Krukonis et al., 2000).

LTTRs comprise one of the largest families of transcriptional regulators in prokaryotes that are involved in diverse biological processes. They are composed of an N-terminal DNA binding domain (DBD) and a C-terminal regulatory domain (RD). Crystal structures of full-length AphB from *V. cholerae* has been determined (Taylor et al., 2012) and comprise a homotetrameric structure that can be described as a dimer of dimers that assembles via two distinct dimerization interfaces, similar to other LTTR proteins.

In *V. cholerae*, AphB was characterized as responsive to intracellular pH and a lack of oxygen (Taylor et al., 2012). AphB takes on an active conformation at low pH or under low oxygen tension, but it remains inactive at high pH (or pH 8.5). Based on AphB crystal structure, the putative ligand binding pocket region was identified, suggesting that the binding of a ligand triggers conformational changes that alter DNA binding (Taylor et al., 2012). An alternative mechanism for AphB was proposed as a thiol-based switch protein, where the thiol is oxidized depending on the presence of oxygen (Liu et al., 2011).

AphB of *V. vulnificus* is not involved with *tcpPH* expression because this species lacks *tcpPH* genes, indicating a different role for AphB in *V. vulnificus* compared to AphB from *V. cholerae* (Jeong and Choi, 2008; Rhee et al., 2006). AphB is known to directly induce *cadC* at the transcriptional level in *V. cholerae* and *V. vulnificus*, which facilitates pathogen survival under acid stress (Kovacikova and Skorupski, 1999; Rhee et al., 2006). Microarray analysis revealed that AphB affected the expression of virulence-involved genes in *V. vulnificus* ATCC 29307, indicating that AphB might be a global regulator contributing to the pathogenesis of *V. vulnificus* (Jeong and Choi, 2008). AphA of *V. vulnificus* does not seem to cooperate with AphB; instead, it is known to upregulate gene expression of the Fe-S cluster regulator *iscR* (Lim et al., 2014). In this study, we determined the crystal structure of the RD of AphB from *V. vulnificus*, followed by functional analyses.

MATERIALS AND METHODS

Construction of the expression vector and protein purification

DNA encoding the AphB RD (residues 88-291) was amplified by PCR using the *V. vulnificus* MO6-24/O genome (accession number CP002469) as a template and was inserted into the expression vector pProEx-HTa (Invitrogen) using NcoI/XbaI restriction enzyme sites. The resulting plasmid (pProEx-HTa-VvAphB-RD) was used to transform *Escherichia coli* strain C43 (DE3) (Miroux and Walker, 1996) for protein production. The *E. coli* strain was cultured in 2.0 L of LB medium including appropriate antibiotics until an OD_{600} of 0.6 and protein production was induced with 0.5 mM IPTG at 30℃. Cells were harvested 5 h after induction, and the cell pellet was resuspended with 50 ml lysis buffer containing 20 mM Tris-HCl (pH 7.5), 150 mM NaCl, and 2 mM 2-mercaptoethanol. After homogenization by French press, the cell lysate was acquired by centrifugation at 13,000 rpm for 30 min. The protein was subsequently purified using a Ni-NTA column and anion-exchange chromatography (HiTrap Q, GE Healthcare, USA). When necessary, the purified protein was incubated with several oxidants at this step. Then, the protein was further purified by size exclusion chromatography (HiLoad Superdex 200 26/600; GE Healthcare) pre-equilibrated with lysis buffer. The final purified proteins were concentrated to 16 mg/ml using a centrifugal filter concentration device (Millipore, USA; 10 kDa cutoff) and stored frozen at -80℃ until use.

Site-directed mutagenesis

The cysteine codon at position 227 (C227) was changed to a serine codon (C227S) using the overlapping PCR method with Pfu polymerase based on pProEx-HTa-VvAphB-RD (Patel et al., 1993).

Crystallization, data collection, and structural determination

Crystallization of the wild type AphB RD and RD treated with the oxidant cumene hydroperoxide (CHP) was performed using the vapor-diffusion hanging drop method at 14℃ under a mother liquor containing 0.1 M HEPES (pH 7.5), 15% (*wt*/*vol*) PEG 8K, and 10% (*vol*/*vol*) ethylene glycol. The crystals were flash-frozen using 25% (*vol*/*vol*) glycerol as a cryoprotectant in a nitrogen stream at -173℃ prior to collecting the X-ray diffraction dataset with the Pohang Accelerator Laboratory beamline 5C (Park et al., 2017) and were processed with the HKL2000 package (Otwinowski and Minor, 1997). Both RD crystals belonged to the spacegroup $P2_12_12_1$, with unit cell dimensions of a = 125.0 Å, b = 188.0 Å, and c = 57.4 Å for the wild type RD and a = 124.8 Å, b = 189.4 Å and c = 57.4 Å for the CHP-treated RD (Table 1). The structure was determined using the MOLREP program in the CCP4 package by the molecular replacement method and a search model taken from the full-length AphB from *V. cholerae* (PDB code: 3SZP) (Winn et al., 2011). The final structure of wild type AphB RD was refined at a 1.9 Å resolution with an R factor of 21.9% and an R_{free} of 26.3% using the PHENIX program (Adams et al., 2010) and the CHP-treated RD at a 2.4 Å resolution. Further details on the structure determination and refinement are given in Table 1.

Crystallization of the AphB C227S mutant RD was performed using the same method as described above with a mother liquor containing 0.35 M potassium thiocyanate (pH 7.0) and 17% (*wt*/*vol*) PEG 3350, and the dataset was collected using Paratone-N as a cryoprotectant. The crystal belongs to the spacegroup $C2$, with unit cell dimensions of a = 230.3 Å, b = 72.4 Å, and c = 112.2 Å. The final structure was refined at a 3.0 Å resolution, and further details on the structure determination and refinement are given in Table 1.

Construction of *aphB* mutant strain

pJR0325, which was constructed previously to carry a mutant allele of *V. vulnificus aphB* on pDM4 (Table 2) (Rhee et al., 2006), was used to generate the *aphB* mutant of *V. vulnificus*. The *E. coli* S17-1 *λpir, tra* strain (Simon et al., 1983) containing pJR0325 was used as a conjugal donor in conjugation with

Table 1. Statistics for data collection and refinement

	Native	CHP-incubated	C227S
Data collection			
Beam line	PAL 5C	PAL 5C	PAL 5C
Wavelength	0.97960	0.97960	0.97930
Space group	$P2_12_12_1$	$P2_12_12_1$	$C2$
Cell dimensions			
a,b,c (Å)	125.0, 188.0, 57.4	124.8, 189.4, 57.4	230.3,72.4, 112.2
α,β,γ (°)	90, 90, 90	90, 90, 90	90, 90, 90
Resolution (Å)	50.0-1.90	50.0-2.40	50.0-3.0
	(1.93-1.90)	(2.44-2.40)	(3.05-3.00)
R_{merge}	0.111 (0.639)	0.122 (0.433)	0.169 (0.445)
I/σI	14.1 (3.7)	13.4 (3.0)	7.2 (2.1)
Completeness (%)	98.1 (85.4)	99.7 (99.4)	97.2 (90.6)
Redundancy	8.7 (6.2)	8.8 (5.7)	4.2 (2.6)
Refinement			
Resolution (Å)	42.26-1.90	45.70-2.40	38.93 - 3.00
No. reflections	90980	51444	28983
R_{work}/R_{free}	0.219/0.263	0.21/0.26	0.24/0.29
No. of total atoms	9655	9382	9186
Wilson B-factor (Å)	19.40	30.79	47.55
R.M.S deviations			
Bond lengths (Å)	0.005	0.003	0.003
Bond angles (°)	1.11	0.56	0.60
Ramachandran plot			
Favored (%)	98.3	97.1	94.9
Allowed (%)	1.8	2.9	5.1
Outliers (%)	0.00	0.00	0.00
PDB ID	5FHK	5X0O	5X0N

Values in parentheses are for the highest resolution shell.
*Values in parentheses are for the highest-resolution shell.
**R merge = Σ hkl Σ i ‖I i (hkl) - [I(hkl)]‖/Σ hkl Σ i I i (hkl), where I i (hkl) is the intensity of the ith observation of reflection hkl and [I(hkl)] is the average intensity of the i observations.
***R free calculated for a random set of 10% of reflections not used in the refinement

Table 2. Plasmids and bacterial strains used in this study

Strain or plasmid	Relevant characteristics [a]	Reference or source
Bacterial strains		
V. vulnificus		
MO6-24/O	Clinical isolate; virulent	Wright et al., 1990
KK1419	MO6-24/O with Δ*aphB*	This study
E. coli		
S17-1λ*pir*	λ-*pir* lysogen; *thi pro hsdR hsdM*$^+$ *recA* RP4-2 Tc::Mu-Km::Tn7;Tp^r Sm^r; host for π-requiring plasmids; conjugal donor	Simon et al., 1983
C43 (DE3)	F$^-$ *ompT hsdS*$_B$ (r_B^- m_B^-) *gal dcm* (DE3) with uncharacterized mutations	Miroux and Walker, 1996
Plasmids		
pProEx-HTa-VvAphB-RD	His_6-tag fusion protein expression vector; Ap^r	Invitrogen
pDM4	R6K γ *ori sacB*; suicide vector; *oriT* of RP4; Cm^r	Milton et al., 1996
pJR0325	pDM4 with Δ*aphB;* Cm^r	Rhee et al., 2006

[a]Tp^r, trimethoprim resistance; Sm^r, streptomycin resistance; Ap^r, ampicillin resistance; Cm^r, chloramphenicol resistance

the *V. vulnificus* MO6-24/O as a recipient. The resulting *aphB* mutant was named KK1419 (Table 2). The conjugation and isolation of the transconjugants were conducted using the method described previously (Jang et al., 2016).

Growth kinetics under acid stress

The wild type and *aphB* mutant strains were grown with LB medium supplemented with 2% (*wt/vol*) NaCl (LBS, pH 6.8) or LBS buffered at pH 5.2 with HCl (DUKSAN, Korea) in 24-well culture plates (SPL, Korea). The cultures were further incubated at 30℃ with shaking for 10 h, and their growth was monitored at OD_{600} with a spectrophotometer (Tecan Infinite M200 reader, Männedorf, Switzerland).

RNA purification and transcript analysis

The wild type and the *aphB* mutant grown to an OD_{600} of 0.5 were exposed to LBS or LBS adjusted to pH 5.2, 6.0 with HCl (DUKSAN) and 7.5 with NaOH (Sigma, USA) for 30 min and harvested to isolate total RNA using the RNeasy® mini kit (Qiagen, USA). For quantitative real-time PCR (qRT-PCR), the concentration of total RNA from the strains was measured using a NanoVue Plus spectrophotometer (GE Healthcare). cDNA was synthesized from 1 μg of total RNA using the iScript™ cDNA synthesis kit (Bio-Rad, USA), and real-time PCR amplification of the cDNA was performed using the Chromo 4 real time PCR detection system (Bio-Rad) with a pair of specific primers (Supplementary Table S1), as described previously (Park et al., 2015). Relative *cadC* and *aphB* mRNA expression levels in the same amount of total RNA were calculated using the 16S rRNA expression level as the internal reference for normalization.

RESULTS

Structural determination of the wild-type AphB regulatory domain from *V. vulnificus*

We initially attempted to obtain the full-length AphB from *V. vulnificus* (*Vv*AphB), but the expression level was not suitable for the ensuing structural study. The RD region (residues 88-291) of the wild type AphB from *V. vulnificus* was successfully produced in the *E. coli* expression system. Rod-shaped crystals were grown at pH 7.5, and a native dataset was collected at a 1.9 Å resolution. The crystals belong to the spacegroup $P2_12_12_1$, and the structure was determined using a molecular replacement model taken from the full-length AphB structure of *V. cholerae*, as previously reported (Taylor et al., 2012). The asymmetric unit of the crystal contains three dimers, resulting in a Matthew's coefficient of 2.11 $Å^3$/Da (Kantardjieff and Rupp, 2003). Similar to the RD structure of AphB from *V. cholerae* (*Vc*AphB), the *Vv*AphB RD forms a stable dimer in the crystal structure (Fig. 1A). Interestingly, we observed that the *Vv*AphB RD had conformational variants among the three dimers in the asymmetric units when superposed (Fig. 1B), with one dimer relatively distinguished from the other two.

Like other LTTR RD structures, the *Vv*AphB RD consists of two subdomains named RD-I and RD-II. The two subdomains are connected through an extended β strand, similar to the *Vc*AphB structure. The N-terminus of RD-I is connected to the DNA binding domain. *Vv*AphB RD monomers are composed of 10 β-strands and 6 α-helices connected by an α/β fold (Fig. 1A).

Structural comparison to AphB from *V. cholerae*

*Vv*AphB and *Vc*AphB share high sequence homology (80% amino acid sequence identity). We found that a *Vv*AphB RD dimer showed a somewhat different conformation from the wild type *Vc*AphB RD (rmsd 0.908 Å between 347 atoms; Fig. 2A), while the other *Vv*AphB RD dimers were very similar to *Vc*AphB (rmsd 0.270 Å between 380 atoms; Fig. 2B).

Importantly, a small cavity was found at the interface between RD-I and RD-II, which was also observed in the

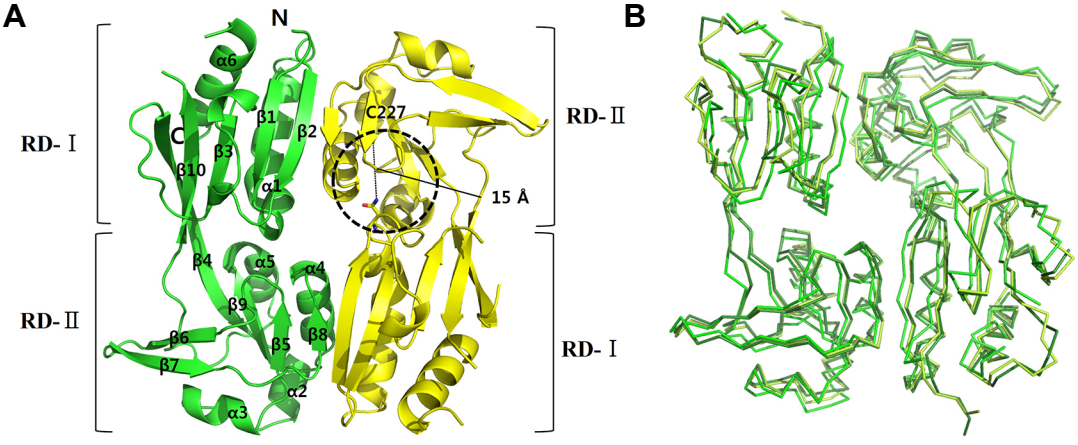

Fig. 1. Overall structure of wild type *Vv*AphB RD. (A) The structure of the wild type *Vv*AphB RD. The two protomers are colored green and yellow. The secondary structures are displayed in the ribbon representations, and the two subdomains (RD-I and RD-II) are labeled. C227 residues are in the RD-II in the second protomer (yellow). A broken-line circle indicates the putative ligand-binding site between the two subdomains. The distance indicates C227 and N100 in the ligand-binding site. (B) Superposition of three dimers from the wild type *Vv*AphB in the asymmetric unit. Each protomer is differently colored.

*Vc*AphB structure (Taylor et al., 2012). In *Vv*AphB, the small cavity was lined with 12 residues, P98, N100, L101, S128, V144, D162, H192, P193, L220, P237, M240, and R262. In the *Vc*AphB, the corresponding cavity was proposed as the putative ligand-binding site despite the fact that the specific co-inducing ligand is not yet known (Taylor et al., 2012). When comparing the residues lining the cavity with *Vc*AphB, the S128 and H192 from the *Vv*AphB RD were substituted in *Vc*AphB with N128 and Y192, respectively (Fig. 2).

C227 in RD-II

We noted the local chemical environment around C227 in RD-II, which is the only cysteine residue in the *Vv*AphB RD (Fig. 1). The cysteine residue is ~15 Å from the small inter-subdomain cavity (Fig. 1). Liu et al. proposed that the cysteine residue senses oxygen level by changing the oxidation state of the thiol moiety (Liu et al., 2011). The role of this cysteine residue is under debate because cysteine residue mutants did not show consistent results (Liu et al., 2011; 2016; Taylor et al., 2012).

To assess the structural impact of the C227 sulfur atom in *Vv*AphB, we determined the crystal structure of a *Vv*AphB C227S mutant variant that was not subjected to oxidation. The crystal belongs to spacegroup *C*2, which is different from the wild type structure, and three dimers are present in the asymmetric unit. The crystal structure was solved at a 3.0

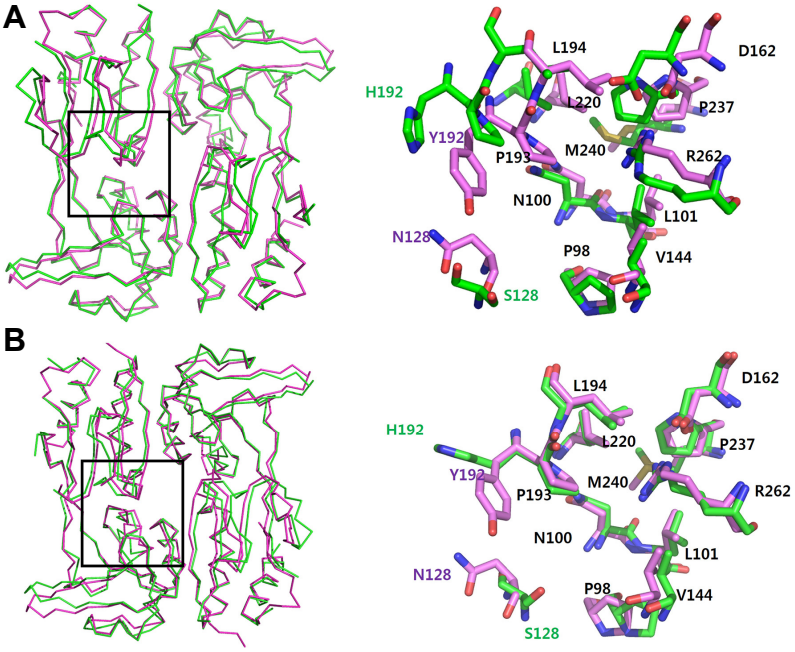

Fig. 2. Structural superposition of wild type *Vv*AphB RD with *Vc*AphB RD. (A) *Vv*AphB RD dimer (green) is superposed onto the wild type *Vc*AphB RD (magenta). (B) The other *Vv*AphB RD dimer (green) is superposed onto the wild type *Vc*AphB RD (magenta). The boxed region in the left panel is enlarged in the right panel that is drawn with stick representations. Each residue is labeled (the common residues in black, with the other residues following the same color scheme) in the right panel.

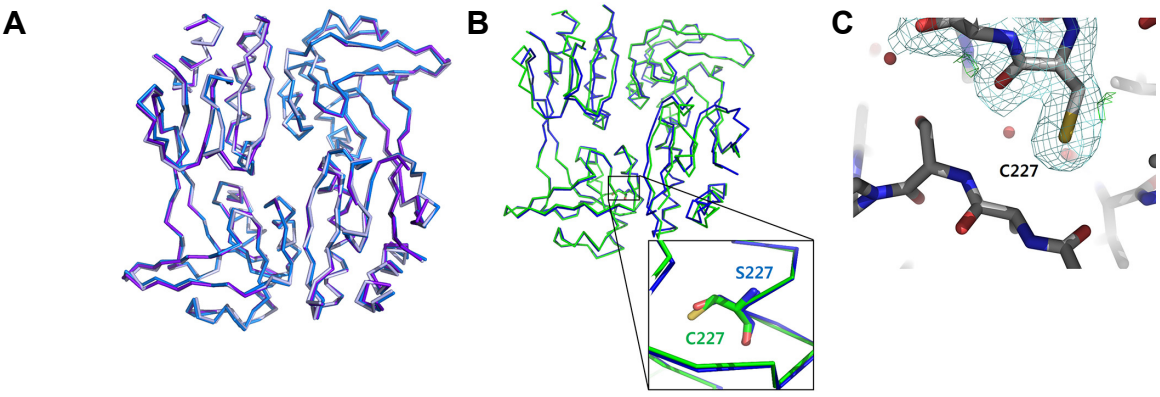

Fig. 3. Structural analysis of the C227 residue in *Vv*AphB RD. Superposition of three dimers from the *Vv*AphB C227S variant in the asymmetric unit. (B) Structural superposition of the wild type *Vv*AphB (green) and the C227S variant (blue) in C-alpha tracing representations. The magnified box shows C227 (or C227S in the variant structure). (C) Electron density maps around C227 in the CHP-treated structure. No modification at C227 was observed. 2*Fo*-*Fc* (pale blue mesh) and *Fo*-*Fc* (green mesh) maps were contoured at 1.0σ and 3.0σ, respectively.

Å resolution by the molecular replacement method using the wild type *Vv*AphB structure. When the three dimers of the mutant protein were superposed, no substantial differences were observed (rmsd 0.496 Å between 328 atoms, rmsd 0.473 Å between 337 atoms (Fig. 3A)). By structural comparison with the wild type *Vv*AphB structure, we found that the two structures were very similar, with a slight difference of the subdomains in the dimeric assembly (Fig. 3B) at the region near the cysteine residue, indicating that the cysteine residue or the sulfur atom might not be important for the function of AphB (Fig. 3B, inset).

A new cavity on the back side of AphB RD

In order to determine reactivity of the cysteine residue, we incubated the crystals with various peroxides such as hydrogen peroxide and alkyl hydroperoxides and determined the structures. No oxidation modification at the cysteine residue was found in the structures under any of the tested conditions (Fig. 3C). In the structure of *Vv*AphB RD treated with cumene hydroperoxide (CHP), we unexpectedly found an unidentified residual electron density map in a different small cavity located at the interface between two monomers on the opposite side of the dimer to the previously known ligand binding site (Fig. 4A). Unfortunately, we failed to identify the compound of the residual density maps since the density maps are rather heterogeneous in the different CHP-treated *Vv*AphB RDs in the asymmetric unit. K103, R104, N221, R224, M240, and Y244 seem to participate in ligand binding (Fig. 4B). suggesting that the cavity might be functionally related. However, further study is required to elucidate the role of the new cavity.

AphB from *V. vulnificus* is activated at low pH and is important for acid tolerance *in vivo*

Both *Vc*AphB and *Vv*AphB contribute to bacterial acid resistance because the known target gene of AphB regulators is *cadC,* which encodes the master positive regulator of the acid tolerance genes *cadA* and *cadB* encoding lysine decarboxylase and cadaverine antiporter, respectively (Merrell and Camilli, 2000; Rhee et al., 2006). In this study, we compared growth kinetics of the wild type *V. vulnificus* MO6-24/O strain and an *aphB*-deleted strain at acidic and neutral pH (pH 5.2 and pH 6.8, respectively). As shown in Fig. 5A, the *aphB*-deleted strain showed a delayed lag phase at acidic pH compared to the wild type strain. At neutral pH, deletion of the *aphB* gene did not affect the growth kinetics. These results are consistent with previous results using *V. vulnificus* ATCC 29307 (Rhee et al., 2006).

We next carried out qRT-PCR to examine pH-dependent AphB transcriptional activity. When we measured *cadC* transcript level in bacteria exposed to pH shock for 30 min, the wild type strain exhibited much higher levels at pH 5.2 and 6.0 compared to pH 7.5 and 6.8 (Fig. 5B). In contrast, the *aphB*-deleted strain was not influenced by external pH; however, the level of *aphB* mRNA was not significantly affected by low pH shock (Fig. 5C). These results suggest that AphB might sense acid shock for *V. vulnificus* and induces the expression of *cadC* and further suggest that the transcriptional activity of AphB protein is changed; however, we note that our findings do not mean that *Vv*AphB directly recognizes acid pH because the external pH variation did not significantly change cytosolic pH, and we cannot exclude the possibility that an unknown pH-sensitive element might affect the activity of AphB.

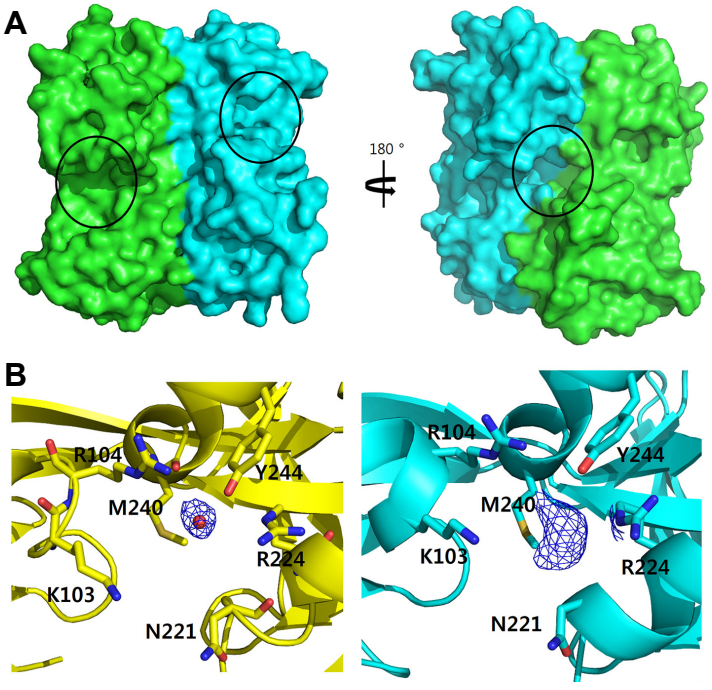

Fig. 4. New ligand binding cavity in the dimeric interface of AphB. (A) The front and back sides of the surface representations of the *Vv*AphB RD dimer. The putative ligand binding sites previously characterized at the interface between RD-I and RD-II are shown in the same orientation of Fig. 1A (left). The newly found cavity is at the interface of the two protomers on the back side of the dimer (right). Each protomer is colored differently (green and cyan), and the putative ligand binding sites or cavity are indicated by black circles. (B) Electron density maps around the newly found cavity between the protomers in the back side of the dimer. While the non-treated structure (yellow) contains a water molecule (red ball, left), the CHP-treated structure (cyan) contains an unidentified molecule displayed by the density map (right). Each of *Fo*-*Fc* electron density maps (blue mesh) were contoured at 1.0σ. Residues in the cavity are displayed in the stick representations.

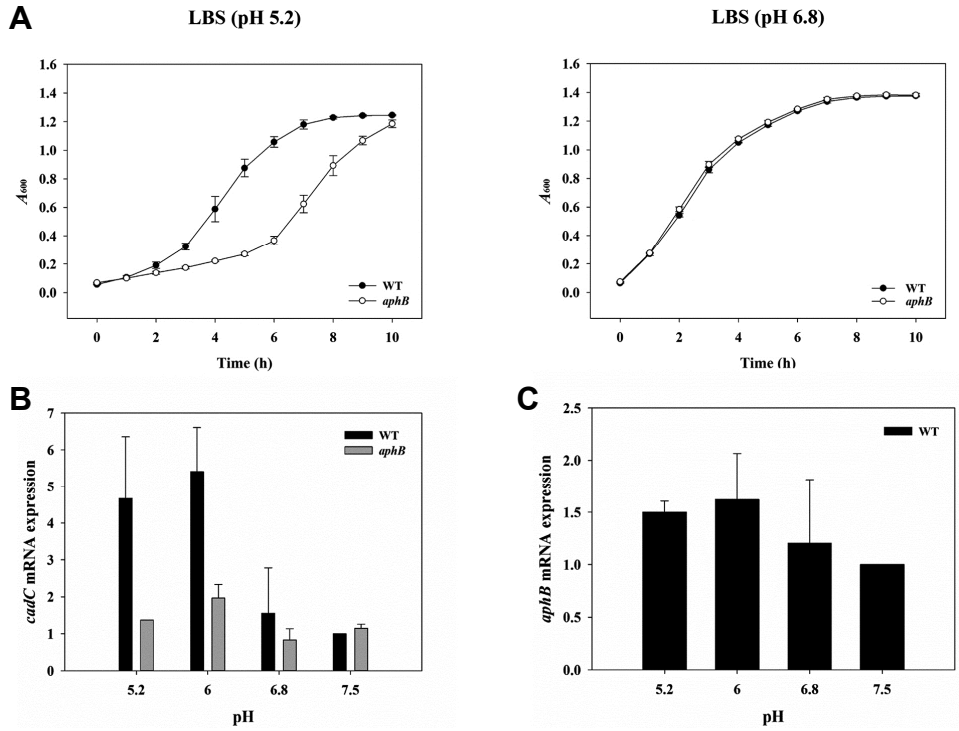

Fig. 5. Effect of AphB on *V. vulnificus* growth and expression of *cadC* and *aphB* under acid stress. (A) *V. vulnificus* strains were compared for their ability to grow in LBS (right) or LBS adjusted to pH 5.2 (left). The result is representative of at least three independent experiments, and the standard deviations (SD) are displayed as the error bars. (B, C) Total RNAs were isolated from *V. vulnificus* cultures grown in LBS or LBS adjusted to pH 5.2, 6.0, or 7.5. The *cadC* and *aphB* mRNA levels were determined by qRT-PCR analyses, and the *cadC* (B) and *aphB* (C) mRNA levels in the wild type grown in LBS adjusted to pH 7.5 were set as 1. Three independent experiments were carried out, and the SDs are displayed as error bars. WT, wild type; *aphB*, *aphB* mutant.

DISCUSSION

In this study, we determined the crystal structures of *Vv*AphB RD under crystallization conditions at pH 7.5. The structure revealed two different conformations similar to those of the wild-type and the constitutive active N100E variant *Vc*AphB, indicating an intrinsic structural flexibility of *Vv*AphB between two states. The putative ligand-binding site in the RD-I and RD-II interface of the front side of the dimer, previously proposed in *Vc*AphB structure (Taylor et al., 2012), was also well defined. Even though it is not clear whether *Vv*AphB operates with the same mechanism as *Vc*AphB, structural resemblance between the two proteins strongly suggests that the same mechanism for sensing those stressful environments are shared.

Since AphB senses anoxic environments, the cysteine residue (C227) was investigated based on the C227S mutant structure and the reaction by various peroxide molecules. The mutation of C227S did not give substantial structural alteration to AphB. Furthermore, incubation of peroxides did not result in any oxidation on the cysteine residue. Instead, the CHP-treated structure showed a new cavity on the opposite side of the RD dimer with an unidentified ligand molecule in it. Taken together, our findings suggest that the cysteine in AphB RD might not directly participate in sensing oxygen.

AphB was responsive to low pH as well as low oxygen tension in *V. cholerae* (Kovacikova et al., 2010; Merrell and Camilli, 2000). Another group performed a mutational analysis of the *Vc*AphB RD by changing amino acid residues lining the cavity to residues with negative charge (P98D, N100E, L101E, P193D, L220E) and revealed that the mutations completely restored the ability of AphB to activate the *tcpPH* promoter at the non-permissive pH of 8.5 in *V. cholerae* (Taylor et al., 2012). The authors proposed that certain residues within the ligand-binding pocket of AphB might be involved in the activity of the protein in response to acid pH. Moreover, our study, together with a previous report (Rhee et al., 2006), strongly suggests that the transcriptional activity of AphB is increased at acidic pH in *V. vulnificus*.

Then, how are the anoxic conditions recognized by AphB in *V. cholerae* and *V. vulnificus*? We noted that the metabolism would be shifted to the anaerobic fermentation producing organic acids, leading to lowering pH in the cytosol when the bacteria are placed under the anoxic condition. Thus it is likely that the anoxic conditions may give the acidic stress to the bacteria. We hypothesized that the ligand for AphB would be a small compound that is accumulated under external acidic or an anoxic stress-induced acidic environment. We don't support that AphB directly sense the cytosolic pH because the cytosolic pH of the bacteria would not substantially change

due to the cellular buffering systems. Instead we believe that the ligand might bind to the ligand binding site(s) of AphB, resulting in the conformational change of AphB. We first paid attention to the CadBA system which antiports cadaverine and lysine across the cell membrane to counteract acidic pH in *V. vulnificus* (Rhee et al., 2005). Given the size of the putative ligand-binding site, an amino acid or its derivative might fit the AphB site. We chose lysine and cadaverine as possible ligands, which are components of the acid resistance system in bacteria. Unfortunately, we failed to determine if lysine and cadaverine bind to the purified *Vv*AphB protein, as judged by the results using isothermal titration calorimetry (data not shown). Although the ligand for AphB was not identified in this study, we suggest molecules in the cellular buffering system as ligand candidates.

In this study, we presented the crystal structures of AphB RD of *V. vulnificus* with the conformational flexibility of AphB. Our findings might exclude the possible mechanism mediated by the cysteine residue in RD, and instead suggests the acidic pH might be more important in activation of AphB. Further studies are still needed to clarify the role and action mechanism of AphB, which help elucidate the virulence mechanism of bacteria at the molecular level.

Note: Supplementary information is available on the Molecules and Cells website (www.molcells.org).

ACKNOWLEDGMENTS

This research was supported by the R&D Convergence Center Support Program (to SHC and NCH) funded by the Ministry for Food, Agriculture, Forestry, and Fisheries, Republic of Korea.

REFERENCES

Adams, P.D., Afonine, P.V., Bunkoczi, G., Chen, V.B., Davis, I.W., Echols, N., Headd, J.J., Hung, L.W., Kapral, G.J., Grosse-Kunstleve, R.W., et al. (2010). PHENIX: a comprehensive Python-based system for macromolecular structure solution. Acta Crystallogr. D Biol. Crystallogr. *66*, 213-221.

Horseman, M.A., and Surani, S. (2011). A comprehensive review of *Vibrio vulnificus*: an important cause of severe sepsis and skin and soft-tissue infection. Int. J. Infect Dis. *15*, e157-166.

Jang, K.K., Gil, S.Y., Lim, J.G., and Choi, S.H. (2016). Regulatory Characteristics of *Vibrio vulnificus* gbpA Gene Encoding a Mucin-binding Protein Essential for Pathogenesis. J. Biol. Chem. *291*, 5774-5787.

Jeong, H.G., and Choi, S.H. (2008). Evidence that AphB, essential for the virulence of *Vibrio vulnificus*, is a global regulator. J. Bacteriol. *190*, 3768-3773.

Kantardjieff, K.A., and Rupp, B. (2003). Matthews coefficient probabilities: Improved estimates for unit cell contents of proteins, DNA, and protein-nucleic acid complex crystals. Protein Sci. *12*, 1865-1871.

Kovacikova, G., Lin, W., and Skorupski, K. (2010). The LysR-type virulence activator AphB regulates the expression of genes in *Vibrio cholerae* in response to low pH and anaerobiosis. J. Bacteriol. *192*, 4181-4191.

Kovacikova, G., and Skorupski, K. (1999). A *Vibrio cholerae* LysR homolog, AphB, cooperates with AphA at the *tcpPH* promoter to activate expression of the ToxR virulence cascade. J. Bacteriol. *181*, 4250-4256.

Krukonis, E.S., Yu, R.R., and Dirita, V.J. (2000). The Vibrio cholerae ToxR/TcpP/ToxT virulence cascade: distinct roles for two membrane-localized transcriptional activators on a single promoter. Mol. Microbiol. *38*, 67-84.

Lee, M.A., Kim, J.A., Yang, Y.J., Shin, M.Y., Park, S.J., and Lee, K.H. (2014). VvpM, an extracellular metalloprotease of *Vibrio vulnificus*, induces apoptotic death of human cells. J. Microbiol. *52*, 1036-1043.

Lim, J.G., Park, J.H., and Choi, S.H. (2014). Low cell density regulator AphA upregulates the expression of *Vibrio vulnificus* iscR gene encoding the Fe-S cluster regulator IscR. J. Microbiol. *52*, 413-421.

Liu, Z., Yang, M., Peterfreund, G.L., Tsou, A.M., Selamoglu, N., Daldal, F., Zhong, Z., Kan, B., and Zhu, J. (2011). *Vibrio cholerae* anaerobic induction of virulence gene expression is controlled by thiol-based switches of virulence regulator AphB. Proc. Natl. Acad. Sci. USA *108*, 810-815.

Liu, Z., Wang, H., Zhou, Z., Naseer, N., Xiang, F., Kan, B., Goulian, M., and Zhu, J. (2016) Differential Thiol-Based Switches Jump-Start *Vibrio cholerae* Pathogenesis. Cell Rep. *14*, 347-354.

Merrell, D.S., and Camilli, A. (2000). Regulation of vibrio cholerae genes required for acid tolerance by a member of the "ToxR-like" family of transcriptional regulators. J. Bacteriol. *182*, 5342-5350.

Milton, D. L., O'Toole, R., Horstedt, P., and Wolf-Watz, H. (1996). Flagellin A is essential for the virulence of *Vibrio anguillarum*. J. Bacteriol. *178*, 1310-1319

Miroux, B., and Walker, J.E. (1996). Over-production of proteins in *Escherichia coli*: mutant hosts that allow synthesis of some membrane proteins and globular proteins at high levels. J. Mol. Biol. *260*, 289-298.

Otwinowski, Z., and Minor, W. (1997). Processing of X-ray diffraction data collected in oscillation mode. Methods Enzymol. *276*, 307-326.

Park, J.H., Jo, Y., Jang, S.Y., Kwon, H., Irie, Y., Parsek, M.R., Kim, M.H., and Choi, S.H. (2015). The *cabABC* operon essential for biofilm and rugose colony development in *vibrio vulnificus*. PLoS Pathogens *11*, e1005252.

Park, S., Ha, S., and Kim, Y. (2017) The protein crystallography beamlines at the pohang light source II. BIODESIGN *5*, 30-34.

Patel, V.P., Rojas, M.R., Paplomatas, E.J., and Gilbertson, R.L. (1993). Cloning biologically active geminivirus DNA using PCR and overlapping primers. Nucleic Acids Res. *21*, 1325-1326.

Rhee, J.E., Kim, K.S., and Choi, S.H. (2005). CadC activates pH-dependent expression of the *Vibrio vulnificus cadBA* operon at a distance through direct binding to an upstream region. J. Bacteriol. *187*, 7870-7875.

Rhee, J.E., Jeong, H.G., Lee, J.H., and Choi, S.H. (2006). AphB influences acid tolerance of *Vibrio vulnificus* by activating expression of the positive regulator CadC. J. Bacteriol. *188*, 6490-6497.

Simon, R., Priefer, U., and Phuler, A. (1983). A broad host range mobilization system for invivo genetic-engineering - transposon mutagenesis in gram-negative bacteria. Bio-Technol. *1*, 784-791.

Taylor, J.L., De Silva, R.S., Kovacikova, G., Lin, W., Taylor, R.K., Skorupski, K., and Kull, F.J. (2012). The crystal structure of AphB, a virulence gene activator from *Vibrio cholerae*, reveals residues that influence its response to oxygen and pH. Mol. Microbiol. *83*, 457-470.

Winn, M.D., Ballard, C.C., Cowtan, K.D., Dodson, E.J., Emsley, P., Evans, P.R., Keegan, R.M., Krissinel, E.B., Leslie, A.G., McCoy, A., et al. (2011). Overview of the CCP4 suite and current developments. Acta Crystallogr. D Biol. Crystallogr. *67*, 235-242.

Wright, A. C., Simpson, L. M., Oliver, J. D., and Morris, J. G. (1990). Phenotypic evaluation of acapsular transposon mutants of *Vibrio vulnificus*. Infect. Immun. *58*, 1769-1773